Available online at www.sciencedirect.com
ScienceDirect
Journal of the European Ceramic Society 30 (2010) 3187–3201
www.elsevier.com/locate/jeurceramsoc

Friction surface evolution of carbon fibre reinforced carbon/silicon carbide (C_f/C-SiC) composites

Yuan Wang, Houzheng Wu *

Department of Materials, Loughborough University, Leicestershire LE11 3TU, UK

Received 10 March 2010; received in revised form 24 June 2010; accepted 9 July 2010
Available online 4 August 2010

Abstract

A study is reported on the development of friction surface of carbon fibre reinforced ceramic composites through microstructural image registration of the surface after a range of braking stops on a laboratory-scale dynamometer test rig. It has been found that a steady friction transfer layer is developed in silicon regions; in carbon fibre/carbon and most silicon carbide regions, the friction surface is unsteady and any possible friction transfer layer is hardly built up with satisfactory longevity. Large voids and cracks/crevices are likely to be filled with transferred materials, but these compacts are susceptible to be stripped off by further braking operation. From this study, three types of friction surfaces are identified and could exist in bedding stage. Under the current testing configuration and regime, coefficient of friction increases with accumulated braking stops, and no stable friction yet appeared. The development of friction surface and its impact on the friction measurements are discussed.

Keywords: A. Composite; B. Fibres; C. SiC; D. Wear parts; E. Friction

1. Introduction

Carbon fibre reinforced ceramic composites have progressively been used as discs, or rotors as some call them, of friction brakes in transport vehicles to benefit from the light weight and long durability that the combination of carbon fibres (as reinforcements) and ceramics (as matrix) can provide when they are appropriately engineered together through tailoring microstructure of the composites.[1] Among these composites, the one with a matrix consisting of carbon and silicon carbide has been mostly exploited; in the real world, silicon could be another constituent of the matrix particularly when silicon infiltration is included in manufacture, whilst this type of composite is frequently abbreviated as C_f/C-SiC.[2–6]

Friction performance of C_f/C-SiC composites has been studied under various braking contexts. It is noticed that the friction behaviour of these composites is in general different from that of metallic materials, e.g. grey cast irons and metal matrix composites, when they are tested against a counterpart, typically an organic or sintered-metallic pad. Such a distinction could lead to particular difficulties in implementing knowledge and experiences that have been accumulated for a long period of time in the development of pad materials for metallic discs; a consequence of this could create a potential impediment in fulfilling the potentials that C_f/C-SiC can provide. A further understanding is therefore needed to underpin possible mechanisms that could govern the observed friction behaviour of C_f/C-SiC composites when they are engaged with pad materials. Such an understanding is likely to provide guidelines for the development of pad materials, and more importantly right now, for any further attempts to optimize the microstructure of C_f/C-SiC composites or their friction bearing surfaces, in order to achieve the required friction and engineering performance of the friction brakes.

Friction performance of C_f/C-SiC composites is normally examined under a disc to pad or disc to disc configuration. It is noticed that the microstructural constituents of the friction surface of the composite disc could have a strong influence on the friction performance and wear resistance. For instance, when the C/C_f-SiC discs were coupled with carefully selected sintered-metallic pads, a higher, more stable coefficient of friction (COF), and a lower wear rate were achieved for the couple with a friction surface of the composite consisting of silicon carbide only than that with a surface containing more than just silicon carbide, such

* Corresponding author. Tel.: +44 1509 223342; fax: +44 1509 223949.
E-mail address: h.wu2@lboro.ac.uk (H. Wu).

0955-2219/$ – see front matter © 2010 Elsevier Ltd. All rights reserved.
doi:10.1016/j.jeurceramsoc.2010.07.019

as carbon, carbon fiber filaments, and silicon.[4] This observation signifies that the inherent microstructure of these composites may provide a complexity of friction surface to accommodate the braking context; some microstructural constituents and characteristics on the surface may have less synergy or even negative effects on the performance of a brake.

It was also noticed that, when such a composite was set to against itself, i.e. disc to disc configuration, the friction performance, including the level of COF and its stability, was improved with the reduction of porosity and the increase of carbon content, and the wear rate became more dependent on the resistance of silicon carbide regions on the thermo/mechanical stresses.[7] Post-mortem examination on the friction surface indicated that no significant friction transfer layer/film was developed, except crumbled carbon and carbon fibre debris. Afterward, same researchers believed that the graphitization of the carbon and the appearance of friction transferred layer on the friction surface might have benefited the improvement in friction performance,[8] whilst a more *ad hoc* analysis is needed to unveil the underpinning reasons at a microstructural level. It was also claimed that C_f/C-SiC composites manufactured by liquid silicon infiltration (LSI) had a higher coefficient of friction and lower wear rate than those manufactured by chemical vapour infiltration (CVI).[3] These experimental observations seem to invoke a need that a further understanding of the friction performance of these ceramic composites should concentrate on what happens at the microstructural level, apart from friction performance evaluation based on engineering tests.

It has been noticed that the counterpart of the composite disc could play a key role as well in determining the level and the stability of coefficient of friction for a specified friction couple. Two kinds of materials have been developed for pads to against the ceramic composite discs, i.e. polymeric material bonded composite (often called organic) and sintered-metallic composite (called sintered). The formulation of the pad materials could lead to a wide range of friction performance by against the same ceramic disc. For instance, when sintered pads were slightly twisted in its formulation, the coefficient of friction could vary from 0.3 for bronze pad with silicate reinforcements, to 0.65 with a further addition of graphite and increase of silicate[9]; Stadler et al. also noticed that softening the sintered pad by adding graphite led to an increase of COF.[10] In the development of pad materials for metallic rotors, one of the major focuses is on the development of friction transfer films on the friction surfaces of both pad and disc. It is believed that a reaction product could be generated on the mating surfaces of the friction couple during friction braking; it is these layers that give the friction couple the expected level and stability of coefficient of friction, and wear resistance. It is well known, for instance, that a friction transfer film with a thickness of from several to tens microns is likely developed when organic/sintered pads are set to against grey cast iron.[11] In our knowledge, little study has however been published on the development of friction transfer film or layer on the surface of ceramic composites disc, though tribological study implies that such a transfer film could be developed under certain conditions. For example, Paris et al.[12] noticed that both steel and alumina ceramic pins could generate an adhering layer on the friction track of C_f/SiC composites; they speculated that it was the difference in the development of the layers and their lifecycle that made the difference in friction behaviour and wear rate.

In this paper, we will systematically observe the development of friction surface in the early stage of braking, which is likely inside the regime of so-called bedding stage of a friction brake. The friction surface will be registered using optical microscopy to illustrate the evolution of friction surface on the composite surface; scanning electron microscopy (SEM) and energy dispersive X-ray (EDX) analysis are also used for any further characterisation of the friction surface. The characteristics and possible developing mechanisms of the friction surface will be generalised and discussed.

2. Experimental procedures

2.1. Testing components preparation

The C_f/C-SiC composites used in this study was supplied by industry. The composites were manufactured through chemical vapour infiltration (CVI) to generate carbon fibre/carbon (C_f/C) preforms first, followed by a liquid silicon infiltration (LSI) process to partly convert the carbon matrix into silicon carbide while the silicon melt were filling into channels among C_f/C regions. The as-manufactured C_f/C-SiC composite blocks were cut into discs in laboratory with a diameter of 50 mm and a thickness of about 15 mm. Two countersink holes with a diameter of 7 mm were drilled on a circular with a diameter of 22 mm on the discs for bolting the tested discs on the sample jig, which is attached to the axle, as shown in Fig. 1.

All testing surfaces of the discs were finished following the same procedure: the as-received surfaces of C_f/C-SiC discs were ground on a grinder (Struers Tegrapol-25, Denmark) with diamond grinding plates starting from a grit size of about 68 μm (220 mesh), then 26 μm (600 mesh), and 15 μm (1200 mesh), with a removing thickness of about 300–400 μm per step; the ground surfaces were polished with 3 μm diamond paste on a polisher (Struers MD Piano grinding disc, Denmark), to ensure any damages left in previous step were completely removed.

Non-asbestos organic (NAO) brake pads were selected in this study. The pads were mounted on a steel back plate in a ring shape with an outside diameter of 48 mm, inner diameter 40 mm, and thickness 12 mm. The surfaces of the pads were ground on a grinding wheel with SiC grits in a size of 3 mm before used for the first braking.

2.2. Friction tests

The friction tests were conducted on a laboratory-scale dynamometer; the schematic diagram of the assembles of the dynamometer is shown in Fig. 1. This dynamometer can provide an inertia of 0.0007 kg m^2 and capability of operation with a rotation speed up to 18,000 rpm and braking force up to 800 N. In each braking test, the C_f/C-SiC disc rotates, with its kinetic energy being provided through a spinning flying wheel driven by an air motor. The gas cylinder and solenoid valve are used to control the engagement of the pad with the spinning disc through an

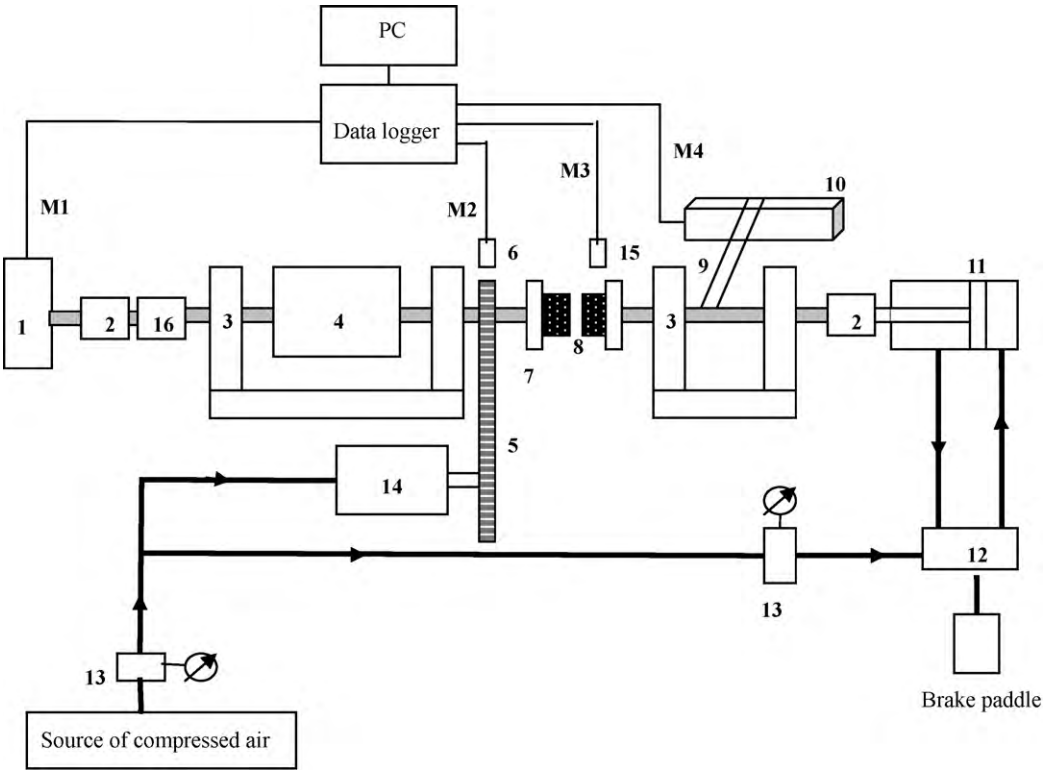

Fig. 1. Schematic diagram of the assembles of a laboratory-scale dynamometer: (1) axle load cell, (2) spacer, (3) stand, (4) flying wheel, (5) gear and belt, (6) angular speed sensor, (7) sample jigs, (8) samples, (9) torque arm, (10) linear load cell, (11) pressure cylinder, (12) solenoid valve, (13) pressure valve, (14) air motor, (15) thermal couple, (16) bearing, (M1) brake load measure, (M2) angular speed measure, (M3) temperature measure, (M4) torque measure.

operation of the brake pedal. The pressure valves are used to control the disc rotation speed and braking pressure. The signals of rotation speed, normal braking load, braking torque and temperature inside the pad, are directly collected by a data logger with a capture frequency of 50 Hz; these signals are then converted into numerical data by a software. Throughout all the tests in this paper, a constant disc rotation speed of $11{,}000 \pm 200$ rpm and a fixed normal braking force of 540 ± 20 N were maintained. The coefficients of friction were calculated using following equation:

$$\mu = \frac{T}{W \times R_e} \tag{1}$$

where T is the braking torque, W the normal braking load and R_e is the effective radius (22 mm here) of friction contacting area. Under the current testing condition, the pad unit pressure is about 0.9 MPa, speed at outside diameter (OD) of the pad ~25,000 mm/s and at inner diameter ~21,000 mm/s; these testing conditions on this small scale dynamometer are comparable to most of the vehicle testing condition.

The measurement of COF was completed on each discrete braking that led the rotating disc to complete still (here, each discrete braking is called one stop). The braking time needed for each stop was about 3 s, and the time interval for the start of next braking after a stop was set as 6 s. For any new setup with both the rotor and pad containing fresh surfaces, an accumulated number of 49 stops were accomplished. In order to follow the development of friction surface, observing points were set after braking stop at the 1st, 2nd, 3rd, 6th, 9th, 14th, 19th, 29th and 49th, where the disc and pad were taken off from the friction testing rig, and re-fixed as they were in the original setup, after completing all examinations. One observation is called here for all measurements between the closest observing points; these measurements included COFs of all stops, and microstructure details on the friction surface after the last stop inside an observation.

To ensure the reliability of the testing data, the same test pattern was repeated up to 4 times using the same C_f/C-SiC disc with its surface being re-finished by following the same procedure after each set of tests.

2.3. Friction surface characterization

The friction surface of C_f/C-SiC at each observing point was examined and registered by imaging the selected regions with optical microscopy (OM) (MeF3, Reichert-Jung, Wien, Austria). The key phases, e.g. silicon carbide, graphite, silicon and carbon fibre filaments were differentiated by the contrast under polarized lighting condition, as long as the original surface was not yet completely covered by friction film. When any other features appeared in OM images, SEM/EDX was used to identify the major chemical elements and microstructure.

Secondary-electron imaging and EDX analysis of friction surfaces were accomplished on a field emission scanning electron microscope (Leo S360, Cambridge Instruments, Cambridge, UK). In most cases, the operating electron acceleration voltage was set to 5 kV; when further information was needed

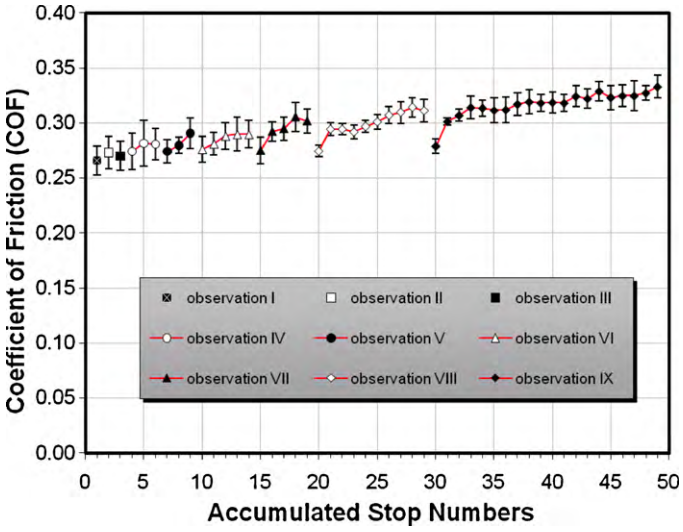

Fig. 2. Measurements of coefficient of friction (COF) against the accumulated braking stop numbers. Each observation includes the 1st stop after refitting the friction couple to that where the couple was dismantled from the rig for surface examination. Observations I–III include one braking stops; other have more than one braking stop.

on the variation of constituents underneath top surface, other voltages could be chosen.

3. Experimental results

3.1. Coefficient of friction (COF)

The measurements of COF are plotted in Fig. 2 against the accumulated braking stop numbers. For each stop, the averaged value, with its standard deviation, is a result of four repeated tests using the same disc and pad materials under the same setup and operating conditions. The results are also grouped into observations as shown in Fig. 2, and measurements inside each observation are linked with a line to show the trend of variation of COF with braking stops.

Inside each observation, the measurements of COF show an ascending trend with the increase of the accumulated braking stops (see observations IV–IX), apart from observation I–III where only one braking stop is included. In any observations consisting of multi braking stops, the first stop gives the lowest COF, comparing to the others following it; the COFs of the first stops in all observations are mostly at a similar level. Among these first brakings, the very first one in observation I has the lowest COF, and the one in observation IX gives the highest value, whilst the average values and standard deviations for both first brakings are inside the ranges of error bars of other first brakings. From observation IV to IX, after same number of braking stops, the COF in the later observation is generally higher than that in previous one. It is also noticed that from observation VII, the second braking clearly boosts the level of COF, and then a gradual improvement is followed for each further braking. Among all observations, none of these shows that the measurements of COF have reached a plateau, an indicator that is usually used to mark the end of bedding process, even in the last observation where most stops were applied.

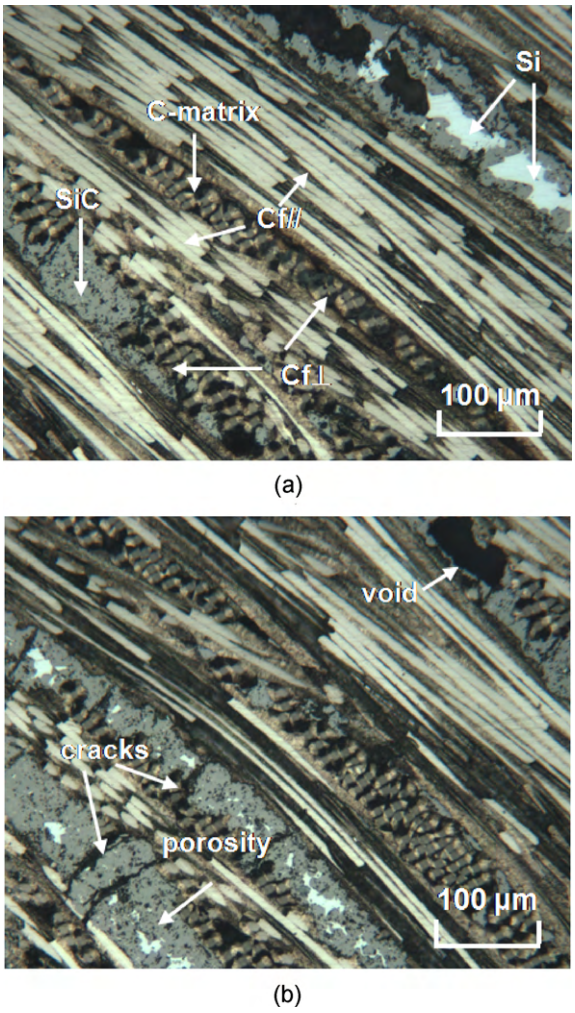

Fig. 3. As-polished surface of C_f/C-SiC disc before braking test. Image in (a) shows two C_f/C regions consisting of in-plane $C_{f//}$ or needled $C_{f\perp}$, large Si and SiC regions between C_f/C regions, and (b) the large cracks across SiC, small porosity and large voids on the polished surface of SiC.

3.2. Friction induced evolution of the surface of the C_f/C-SiC composite

3.2.1. Overview of as-polished surface

The OM images of an as-polished surface are shown in Fig. 3. Two types of oriented carbon fibres exist on the surface: nearly in-plane fibres ($C_{f//}$) with fibre lay-out being inside or slightly off the friction plane, and nearly perpendicular fibres ($C_{f\perp}$) with fibre directions nearly perpendicular to friction surface. The former accounts for the majority of the fibres exposed on the surface, and the later is believed to be the needling fibres for holding the fibre laminae together. Both types of fibre orientation are shown in Fig. 3(a), as marked. Around each fibre filament, a layer of carbon is surrounded; these carbon regions show bright and dark contrast under polarized lighting condition, which might indicate that the carbon matrix could be a graphite region with

fairly uniform structure (n.b. we will hereafter call these regions carbon, carbon matrix or C-matrix with no implication of any particular crystallography of carbon). Among the fibre bundles bonded and embraced by the carbon matrix, there exist silicon carbide and silicon regions, which show grey and white contrast, respectively. In microstructural aspect, voids with a size scale up to tens microns and large cracks/crevices exist on the as-finished surface, as well as small porosity within a scale of a few microns, inside both SiC and carbon regions, as shown in Fig. 3(b). In summary, the friction surface is composed of

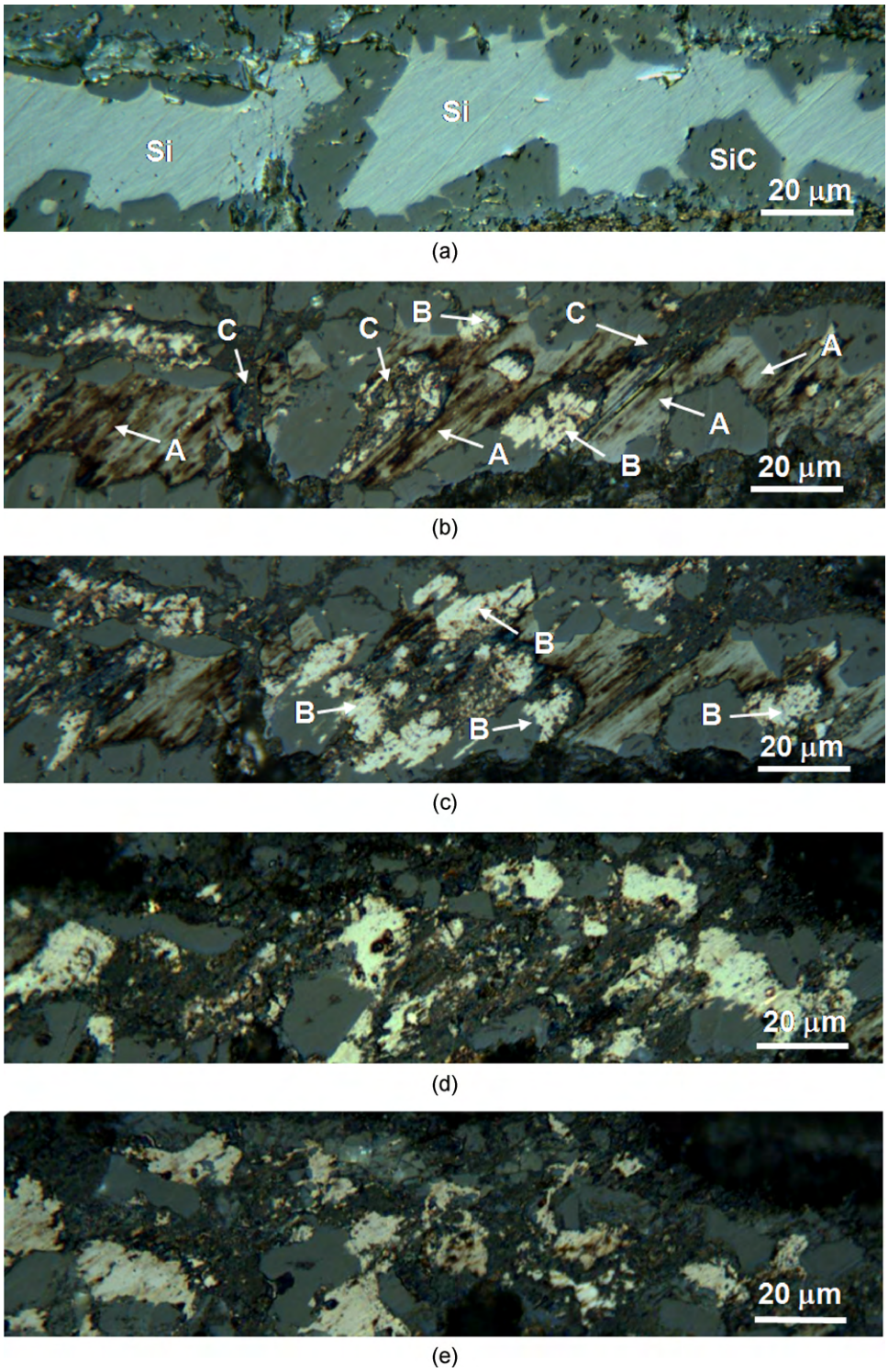

Fig. 4. Registered OM images to illustrate the development of friction surface in silicon regions of the composite: (a) as-finished surface in silicon regions before braking test; (b), (c), (d) and (e) the surface after the 2nd, 3rd, 19th and 49th braking stop, respectively. The arrowed areas are categorized as type A, type B and type C friction surface that consists of friction transferred layer on top and displays a contrast of brownish, white, and dark grey or a mixture of dark grey and white, respectively. (For interpretation of the references to colour in this figure legend, the reader is referred to the web version of the article.)

a structure with a clear hierarchy arrangement of multi phases, along with voids/porosity, large and micro-cracks.

3.2.2. Surface evolution in silicon regions

A series of registered OM images in Fig. 4 show the development of friction surface in a silicon region. With the increase of accumulated numbers of braking stop, a friction transfer film or layer has been built up continuously on the top of this region. Under the current imaging condition, the friction surface after two stops shows three types of contrast: type A in brownish (or light grey in black and white printing), type B in bright white, and type C a mixture of dark grey and white or dark grey only, as marked in Fig. 4(b); it is evident that type A film prevails on the friction surface, whilst type B and C exist in isolated patches. By increasing one more braking stop, more type B and type C patches appears, with a significant shrinkage of type A area, as arrowed in Fig. 4(c). Up to 19 stops, type A contrast is observed in scattered small areas only, but type B and C predominate the friction surface (Fig. 4(d)). By further increasing the number of braking stop to 49, the friction surface shows predominant type B and C contrasts (Fig. 4(e)).

In order to examine the chemical composition of the friction surface where three different contrasts appear under OM imaging condition, low-voltage SEM-EDX analysis was implemented on the surfaces. SEM images and corresponding EDX spectra from areas with different contrasts are summarised in Fig. 5. The friction surface with type A contrast is copper-rich, comparing to other areas; type B is iron rich, and type C contains both copper and iron in a significant amount, as indicated by the intensity of the L lines of Fe and Cu in the EDX spectra. Inside the type A and type C, there exists a significant amount of magnesium and oxygen, while in type B, both oxygen and magnesium are in a very low level, if any. It is yet impossible to confirm whether the existence of oxygen is related to the appearance of other elements, e.g. copper/magnesium, at the current level of characterization. The morphology of the friction surface (actually the friction transfer film or layer, as the chemicals on the surface are different from the composites already) can be differentiated among these three types from the secondary-electron images: both the type A and C look a bit of crumbling with visible granulated materials in the film, though the size of the crumbles in the type A is much smaller than in the type C; the type C has a rougher surface, comparing to the type A, with the existence of craters, voids and cracks. In contrast to the type A and C, the type B film has a smoother surface with much fewer visible particles and voids.

3.2.3. Surface development in silicon carbide regions

The friction surface development in silicon carbide region is shown in Fig. 6. Under an imaging condition of differential interference contrast (DIC), a number of small voids/craters are highlighted on the polished surface of this region (see Fig. 6(a) and Fig. 2). Right after the first braking stop, some of these voids/craters are filled with transferred materials showing dark contrast, as shown in the arrowed sites, and a few in bright contrast; they are marked as type B and C respectively in Fig. 6. After 6 braking stops, these type B patches grow up to a larger

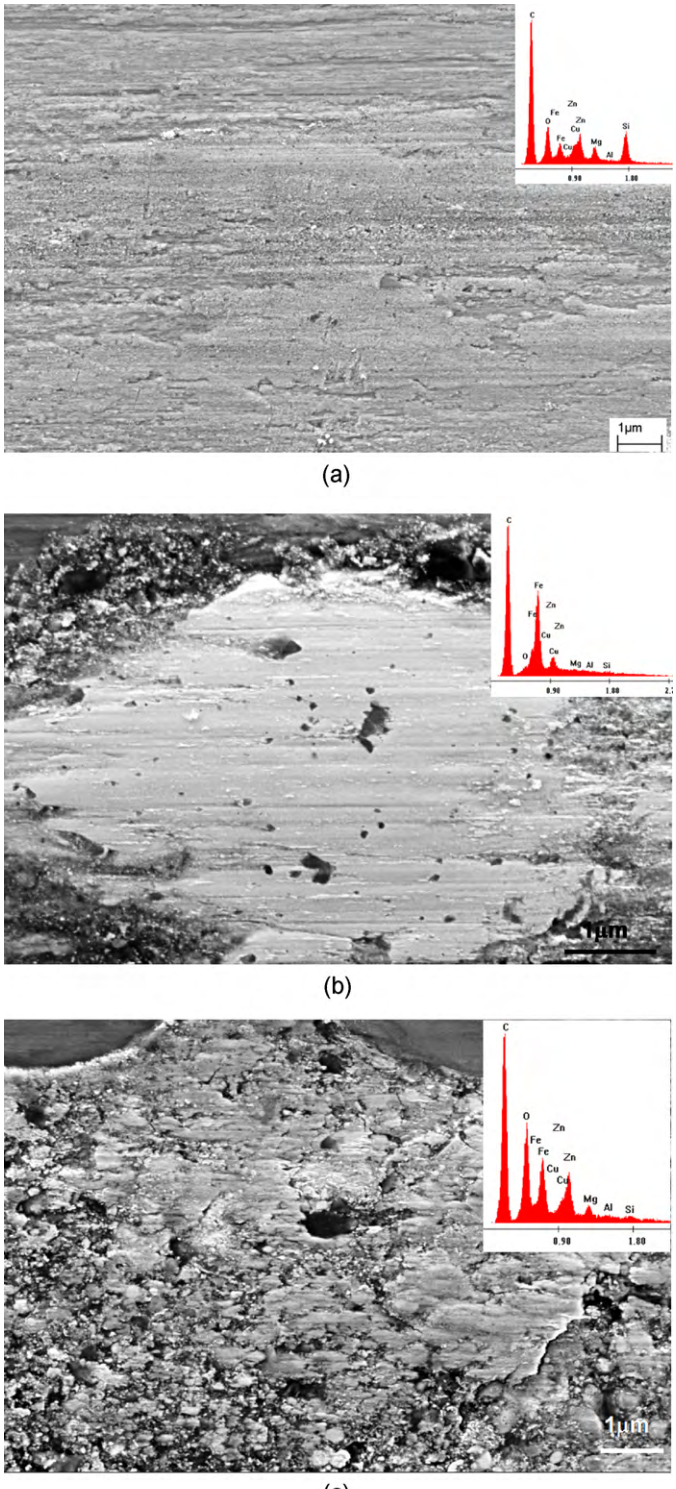

Fig. 5. Secondary-electron images of silicon regions where three types of friction surface appeared in OM imaged (see Fig. 4(b)) when the composite disc was subjected to two braking stops: (a) region with brownish contrast (type A); (b) regions with white contrast (type B); (c) region with a mixture of grey and white colour (type C). Inset in each image is the EDX spectrum obtained from this region under an accelerating voltage of 3 kV. (For interpretation of the references to colour in this figure legend, the reader is referred to the web version of the article.)

extend, and small parts of the type B convert into type C alike, as shown in Fig. 6(c). Subjected further braking stops, these large white patches, along with the small white spots appear in the middle area in Fig. 6(c), are partly or completely covered with type C contrast layers, as seen in the surface images in Fig. 6(d), (e) and (f) after 14, 19 and 49 stops, respectively. Note, no type A contrast area is observed on this friction surface.

It is noticed that after the first stop, the friction surface near the boundary of the silicon carbide region shows type C contrast and a crumbling appearance. When braking stop number increases, such kind of friction surface develops continuously toward the

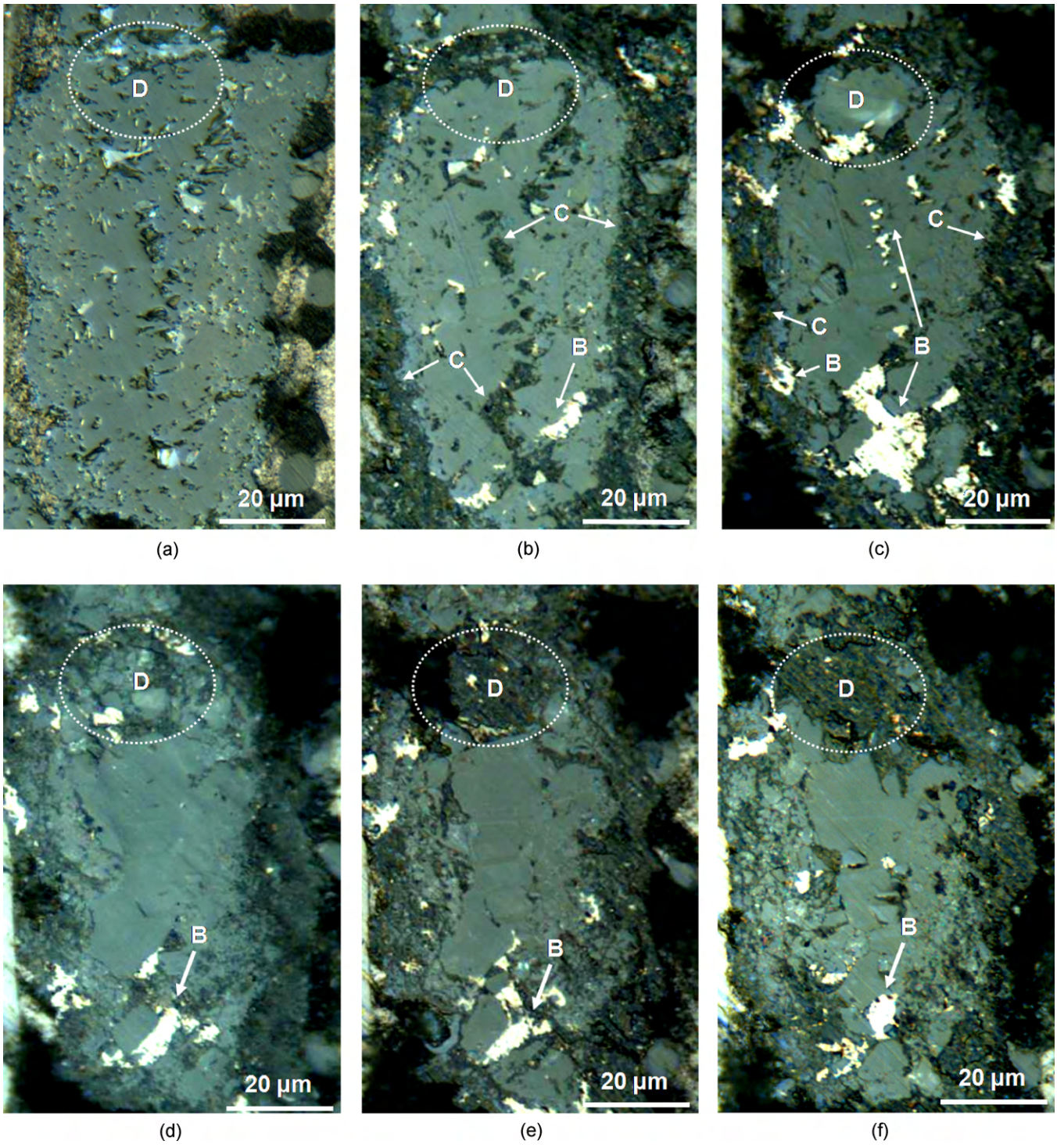

Fig. 6. Registered OM images on the friction surface of a silicon carbide region: (a) as-finished surface before braking; (b), (c), (d), (e) and (f) the friction surface after the 1st, 6th, 14th, 19th and 49th braking stop, respectively. The arrows indicate places where transferred materials were deposited; B and C represent the type of friction surface showing similar contrast as type B and type C friction surface appeared in Fig. 4; D is an area highlighted to notice the journey of the mechanical damage followed by a deposit of transferred materials on SiC surface.

central area of the region. After 49 stops, most of the friction surface in the SiC region shows type C contrast, as shown in Fig. 6(f). It is also noted that before type C appears on the friction surface, extensive cracking has occurred on the SiC surface; some surface area tends to chip off due to lateral cracking. Up to the braking numbers of current test, only the core of this region seems to be in good integrity without clear change of image contrast.

It is worth noting that the development of a circulated region D in the upper part of this area. Images from (a) to (f) show a lateral cracking has been developed underneath the surface in region D between the 1st and 6th stop, and then the partially-detached surface is crushed into many pieces with transferred materials filling in the cracks between the 6th and 14th stop; up to the 19th stop, the whole area is converted into a region completely filled with transferred materials, with a typical type C contrast; to the 49th stop, the area filled with transfer material has expanded further (see Fig. 6(f)).

This SiC region was further analyzed with SEM/EDX after 49 stops (Fig. 7). The EDX measurements confirm that the region is covered or filled with transferred materials. The transferred materials showing type C contrast are composed of iron, cupper, magnesium and oxygen; the region with white contrast is dominated with iron, as shown by the EDX spectrum at position a and c respectively in Fig. 7(a), which should be a further confirmation of the transfer layer belonging to the type B. In the middle area, there is no evidence to show that any transferred material has been deposited on the surface of silicon carbide, as the EDX spectrum shows no more than carbon and silicon lines in position b. However, in another region, EDX spectrum shows that transfer film has deposited on the surface of silicon carbide, though very thin, as shown in Fig. 7(c). Under a higher magnification on the damaged region with type C contrast (Fig. 7(b)), the transferred materials are exposed, and clearly they all fill inside surface cracks; the surface region looks like granulated silicon carbides, with a size ranging from sub-micron to a few microns, that are held together by the transferred materials on the surface.

3.2.4. C_f/C region containing vertical carbon fibres ($C_{f\perp}$)

After first braking stop, the carbon matrix is subjected to significant mechanical damage, and simultaneously the damage areas are filled with transferred materials or/and crumbling particles; same situation occurs on the interfaces between vertical carbon fibres and carbon matrix, as shown in Fig. 8(b). However, the vertical carbon fibres themselves are still in good position. After 49 brakings, majority of the region, including carbon fibre and carbon matrix, has been damaged, and left with transferred materials, as shown in Fig. 8(c). There is no clear type B and C contrast that could be differentiated under the imaging condition. Further SEM/EDX analysing results, as shown in Fig. 8(d), indicate that the voids formed by surface cracking are filled with wear debris with chemical constituents that are typical for transferred film with type C contrast observed on the friction surfaces of silicon and silicon carbide. On the cross-sectional surface of carbon fibres, the smooth and flat part has no transferred materials deposited, as confirmed by the EDX spectrum at position B, so does the exposed carbon matrix surface. It is also noticed that some transferred materials also fill in the damaged interface between carbon matrix and carbon fibre.

3.2.5. Surface development in C_f/C regions containing in-plane carbon fibres

Like the vertical carbon fibres, all in-plane fibres are surrounded with carbon matrix (Fig. 9(a)). After initial braking, fracture occurred in both carbon fibres and carbon matrix, as marked in Fig. 9(b); some fractured parts have been dislodged and stripped away, and the left positions are filled with transferred materials. When more brakings are applied, the more carbon fibres and matrix are dislodged through fracturing, the more are transferred materials deposited on the friction surface, as shown Fig. 9(f). It is noted that all the transferred materials in $C_{f//}$C region look fairly crumbling, lack of enough cohesion. SEM analysis shows that the transferred materials have the same chemical composition as that with the type C contrast in silicon and silicon carbide regions; on the exposed surface of carbon fibres and matrix, there is no transferred material deposited, as shown in Fig. 9(f).

3.2.6. Surface development in large voids and cracks/gaps

Fig. 10(a) shows a typical large voids on the as-polished surface. After one braking stop, the void is completely filled with transferred materials; they look fairly dense. After further braking, some of the filled materials are pulled out. As the braking is kept going, it seems such regions undergo a process of filling-in and partially-dislodging. As seen in Fig. 10(d), the same void is fully filled with transfer materials again. Fig. 11 shows that cracks in silicon carbide regions on the as-prepared surface are also filled by transferred materials fairly swiftly during braking. A similar dynamic process of filling-in and partially-dislodging is observed as that appeared in other large voids.

4. Discussion

The development of the friction surface on the surface of C_f/C-SiC composite is systematically examined through a series of microscopic image registrations on microstructurally representative regions where friction braking is initially executed on an as-machined state by using an organic pad. The knowledge on what may happen on the surface during braking could give a more inclusive understanding of the development of friction surface through physically interacting between the transferred materials produced by the friction operation and the composite that is likely composed of different ceramic constituents and microstructural characteristics. Such an awareness could also light up possibilities of enhancing the overall engineering performance of brakes that consist of ceramic composites through optimising the microstructure of the composites, surface engineering, and fine-tuning of pad materials. By using the experimental results, we will give further analysis and possible generalisation on the circumstance of friction surface, governing factors on its development, and possible correlations between COF and friction surface.

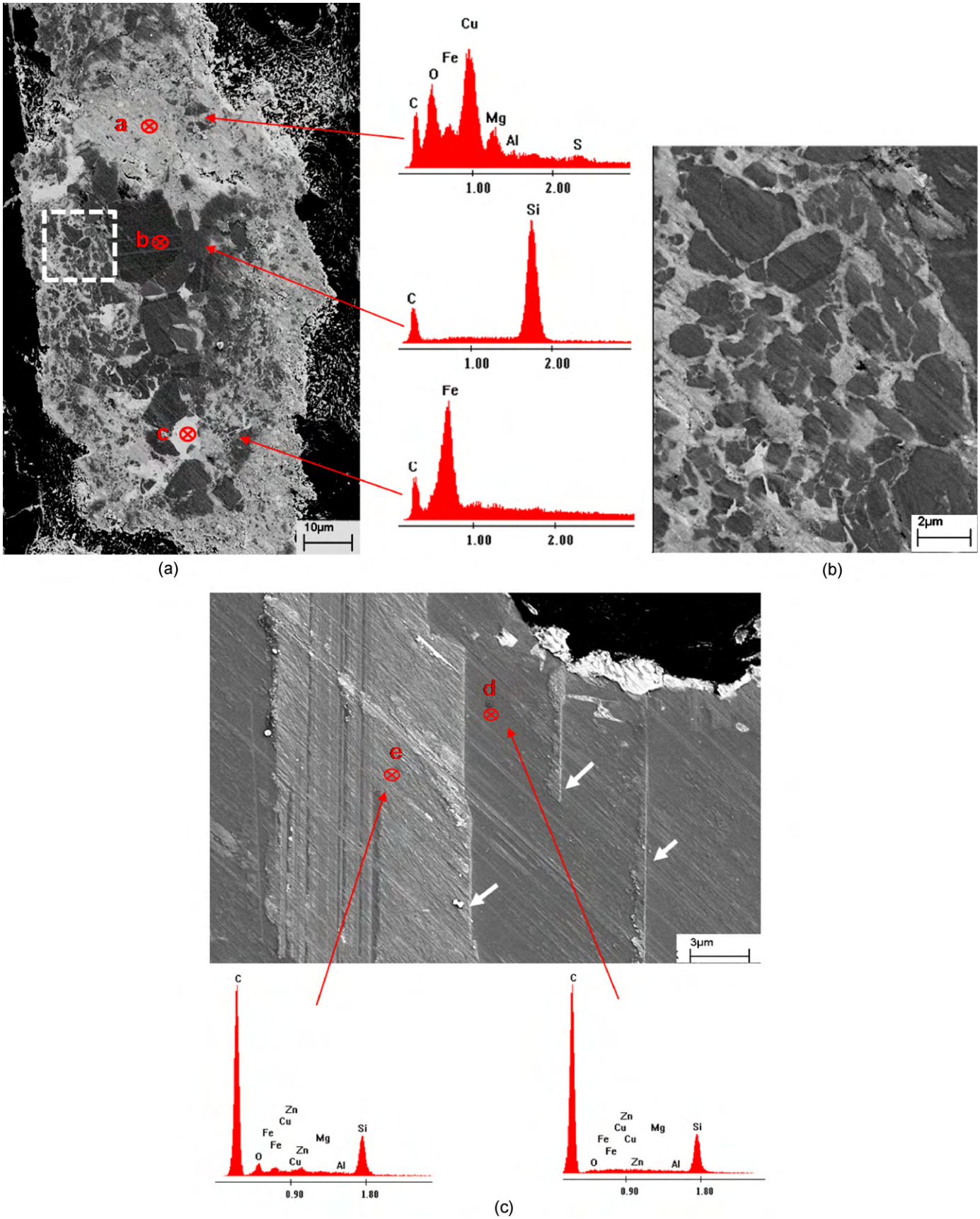

Fig. 7. Secondary-electron images of the friction surface in silicon carbide region after 49 braking stops: (a) a region corresponding to Fig. 6(f) imaged by OM, and EDX spectra in position a, b and c; (b) higher magnification of a region inside a square with dashed line in (a); (c) another silicon carbide region where EDX spectra at position d and e indicate that transferred materials have been successfully deposited. Accelerating voltage was 3 kV for imaging and EDX spectra acquisition.

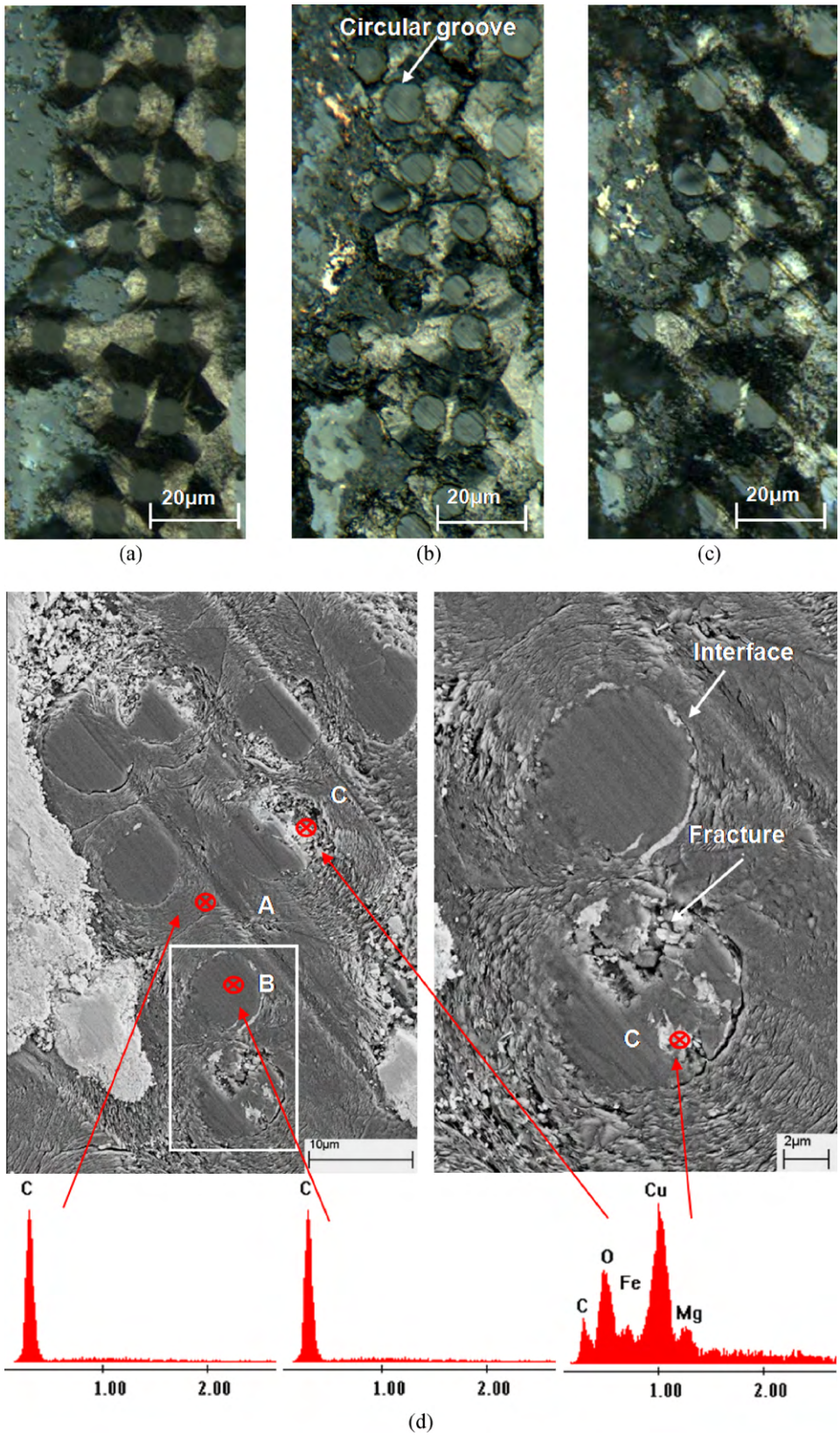

Fig. 8. Registered OM images of the friction surface in a $C_{f\perp}$/C region of the composite: (a) as-finished surface before braking; (b) and (c) the surface after the 2nd, and 49th braking stop, respectively. The arrows indicate a position where circular groove was generated along the interface between $C_{f\perp}$ and carbon matrix after two braking stops. (d) The secondary-electron image of the friction surface in $C_{f\perp}$/C region after 49 braking stops; wear debris accumulated in voids created by fracturing and dislodging, and split interfaces. Spectra from positions A and B indicate no transferred materials being deposited on the surface of carbon matrix and the cross-section surface of carbon fibre; spectrum from position C indicates that deposited debris in voids/gaps contain Cu, Fe, Mg and O.

4.1. The morphology of the friction surface and its development

Registered microscopic images on post-braking surfaces have revealed that transferred materials, or sometimes called third bodies,[13] are introduced onto the surface of the ceramic composites by the braking operations, when a pad, composed of resin bonded materials such as metals and minerals, is used to against the ceramic disc. These third body materials are observed on the friction surface right after the initial braking, regardless the constituents and the microstructure features on the surface of the composite, as shown in Figs. 4(b), 6(b), 8(b), 9(b), 10(b)

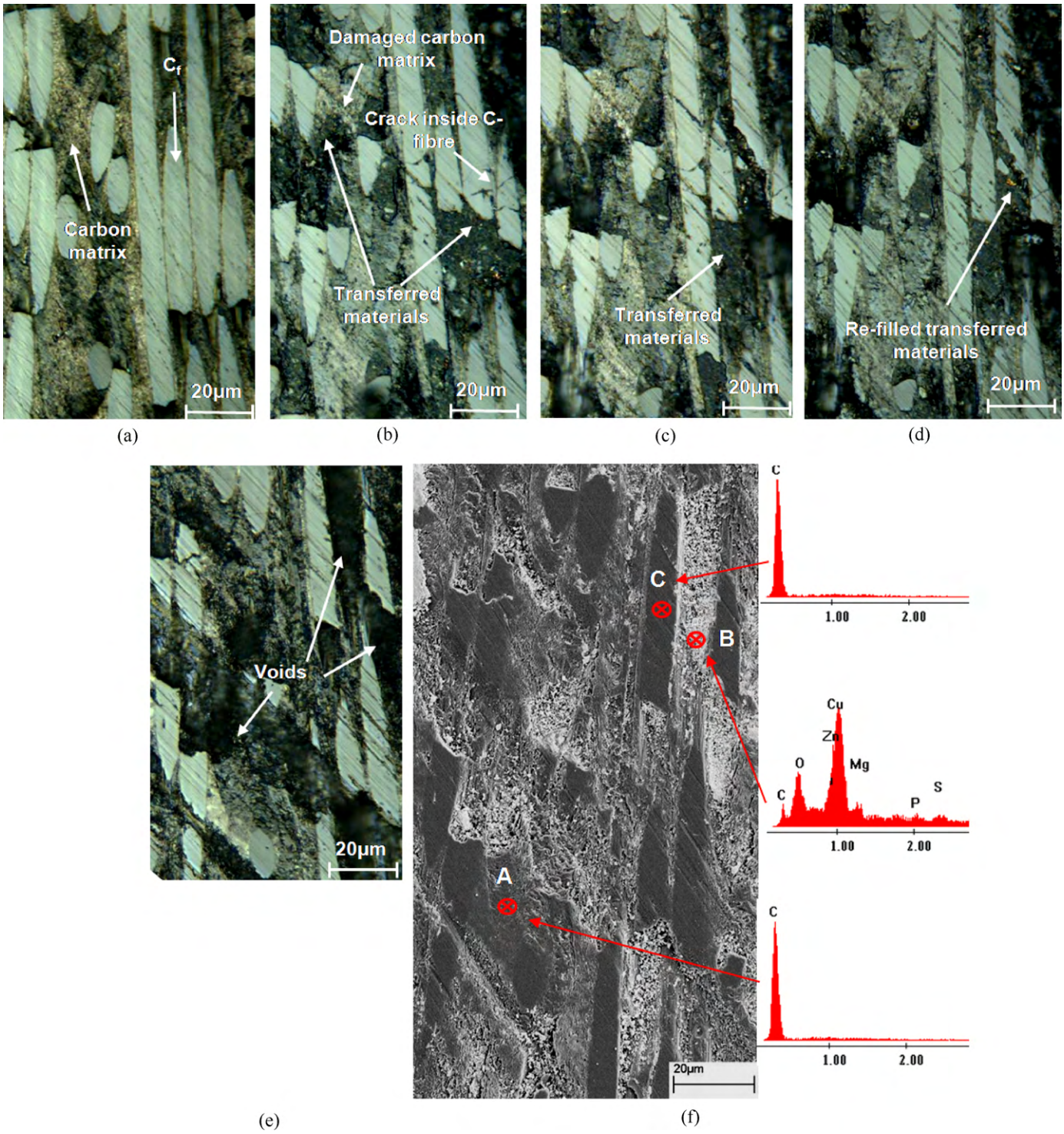

Fig. 9. OM images of friction surface in $C_{f//}$/C region: (a) as-finished surface before braking, (b) after 1 stop, (c) after 2 stops, (d) after 3 stops, (e) after 49 stops. Secondary-electron image and EDX spectra are presented in (f) for the friction surface after 49 braking stops; no transferred materials are identified on the surface of carbon fibre and most of the carbon matrix.

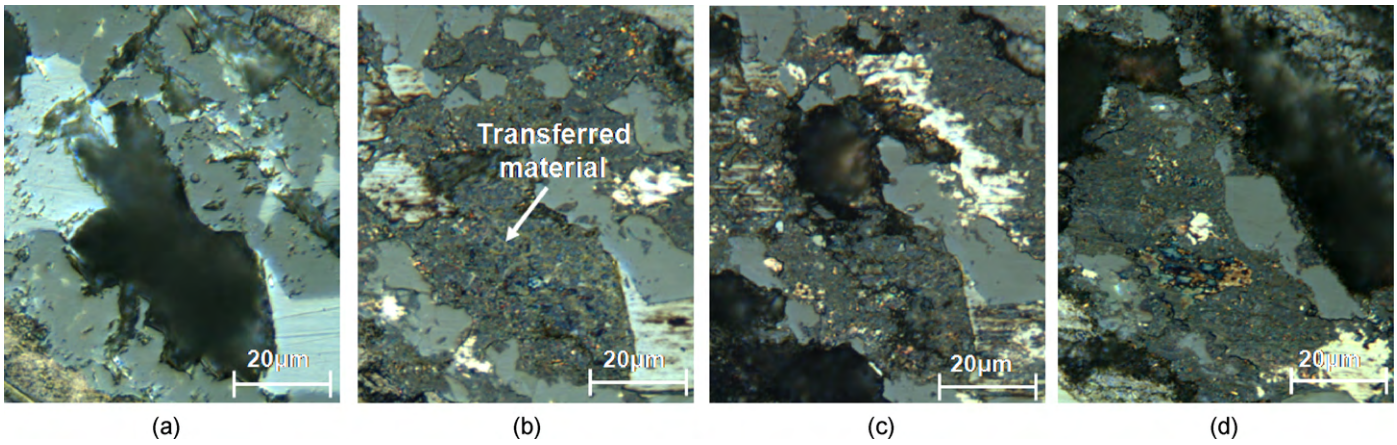

Fig. 10. OM images the friction surface in voids: (a) as-finished before braking, (b) after 1 stop, (c) after 3 stops, (d) after 49 stops.

and 11(b). However, their embedding configuration and existing morphology vary greatly on the surface. On the top of the silicon, the deposition of the transferred materials could be on anywhere of the as-finished surface spreading across the whole region. For silicon carbide, the transferred ones tend to embed in wherever that is topographically lower, e.g. micro-cracks, pits, voids and porosity; these microstructural feature are likely generated by the Hertizan contacting damage of abrasives during surface machining and friction braking, or borne inside the composites themselves. In the C_f/C region, the depositing tendency of the transferred materials is very similar to that observed on silicon carbide. Certain embedding places are nevertheless believed to be created immediately after the friction contact through a possible process of fracturing first, and then dislodging of the materials; these sites can be distinguished by comparing the friction surfaces after 1–3 braking stops (Figs. 8(b) and 9(b)–(d)) with the as-finished ones (Figs. 8(a) and 9(a)). For pre-existing large voids and cracks/gaps, despite their existing locations, they are all filled with transferred materials immediately after the initial brakings. It is believed that the structural features of the voids/cracks/gaps on the surface could provide these regions a function just like a cheese grater does, and the cavities might have collected most of the filled materials that were chipped off from the pad, as seen in Figs. 10 and 11. Note, judging from the appearances of the compacts in Figs. 10 and 11, their density, cohesion and their longevity may vary a lot with the nature of the cavities/gaps, i.e. their depths, in-plane dimensions, shapes and materials surrounding them. We believe that a further study

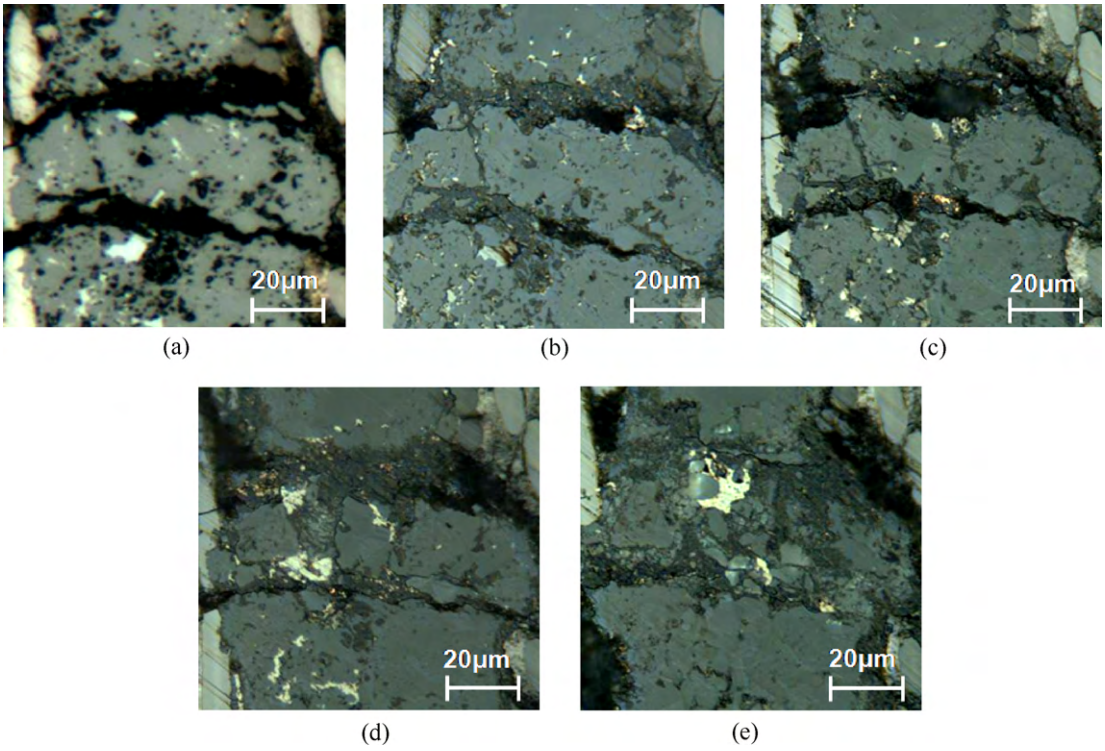

Fig. 11. OM image of friction surface on cracks: (a) as-finished surface before braking, (b) after 1 stop, (c) after 3 stops, (d) after 9 stops, (e) after 49 stops.

would be required on the compacting behaviour of the filled materials if any filling-ups of physically low sites is to be purposely adapted to modify the friction/engineering performance of the composites, whilst some industry successes are claimed in this aspect.

After the preliminary deposition of the transferred materials and any further development in the following up braking, the morphology of the friction surface has subjected to a fairly dissimilar route in different regions; details on the development have been described in last section. Based on the observations, three types of friction surface can be generalized in the early stage of braking, and we categorize them as following:

(a) *type I*, the transferred materials have a relatively stable relationship with the matrix, and any cumulative development should involve an interaction with the previously deposited materials and be able to maintain their longevity in a friction transfer layer;
(b) *type II*, the transferred materials have unstable relationship with the matrix, and the longevity of the friction transfer layer is likely dependant on the durability of the interface between the transferred materials and the matrix, as well as the sturdiness of the near-surface region of the matrix;
(c) *type III*, the transferred materials have a relatively stable relationship with the matrix, but the longevity of the friction transferred materials is likely determined by the cohesion of the compact.

The registered images have revealed that transferred materials are able to successfully deposit on silicon regions and the friction surface consisting of the developed layer should belong to the type I; friction surfaces with those transferred materials on the silicon carbide and on the C_f/C regions can be categorised into the type II; the trapped materials in large voids/gaps existing on the surface should fit in the type III.

4.2. Main factors that could govern friction surface development

In the silicon region, it is noticed that the transferred materials can deposit on the surface straight as long as the pad has a direct contact with the surface of the composite; transferred materials introduced by the following up brakings are likely fused with the previous ones to generate a so-called friction transferred layer over the substrate. Judging from the observed variation in contrast of the OM images on the post-braking surfaces inside silicon regions (Fig. 4), together with the corresponding results of chemical constituent analysis (Fig. 5), we believe that a relatively stable transfer layer might have been built up layer by layer through a fusion of metallic materials and a dispersion of minerals inside them during each braking operation, following the appearance of an initial metallic layer right on the top of silicon, which seems to be strongly bonded. This inference is similar to the observed development of transfer layer on the surfaces of friction couples consisted of grey cast iron rotor and organic pad.[14,15] Further details on the bonding of the initial materials with the silicon, the microstructure of the transfer layer and its building up procedure can be identified and reconstructed with cross-sectional TEM analysis, but this is out the scope of this paper. It is worth mentioning, however, that two factors might be the essential for the successful development of type I transfer layer: first, the initial deposition of transferred materials must have a stable relationship with the substrate; secondly, the substrate must be able to keep its integrity during braking. The former one could be realized through a strong bond between the transferred materials and the substrate; in these silicon regions, our recent analysis has shown one of the bonding possibilities is through a fusion of cupper and silicon under high temperatures generated by the friction.[16] The later one is confirmed by the current observation that in the braking testing regime, no visible fracture damage of the silicon substrate has yet been seen up to the last braking.

In silicon carbide and carbon fibre/carbon regions, the development of transfer layer shows a tendency to be influenced by the unsteadiness of the substrate, if not the lack of strong bonding or adhesion only between the transferred materials and the surface of carbon and silicon carbide. Surfaces in both regions are subjected to breaking damage from the very early brakings, as shown in Figs. 7–9; such damage could obviously lead to an unstable subsurface region. The argument could be that if the transferred materials had had a better adhesion with the substrates and/or the substrates had a higher fracture resistance, the surface of the substrates could have suffered less contact damage and then been able to hold up the transfer layers. Under the current observations, no evidence shows that the transferred materials have a strong adhesion with silicon carbide and carbon, whereas a firm support on the inference can only be done by further TEM analysis. The appearance of significant contacting damage in both silicon carbide and carbon regions implies one possibility that the critical energy releasing rates of silicon carbide (G^C_{SiC}) and carbon (G^C_C) could be lower than that of silicon (G^C_{Si}) in this composite, i.e. $G^C_{SiC} < G^C_{Si}$ and $G^C_C < G^C_{Si}$.

Fracture releasing rate, G^C, is a parameter used to gauge the fracture tolerance of a material under loading condition. It should have the following relationship with the Young's modulus, E, and fracture toughness, K_{IC}, of a material

$$G^C = \frac{(1-\nu^2)K_{IC}^2}{E} \tag{2}$$

where ν is its Poison ratio. By re-arranging Eq. (2), we should have the following linear relationship between logarithm of modulus and fracture toughness.

$$\log_{10}\ K_{IC} = \frac{1}{2}\log_{10}\left(\frac{E}{1-\nu^2}\right) + \frac{1}{2}\log_{10} G^C \tag{3}$$

In a $\log_{10}(K_{IC})$–$\log_{10}(E/1-\nu^2)$ chart, the intercepts on the K_{IC} axis of parallel linear lines with a slope of 1/2 represent the values of G^C. A group of such lines have been drawn in Fig. 12, with specific values are labelled for the fracture strain rates. When materials sit on the same line, it indicates that they should have same fracture strain rate; materials near the top left corner should have larger fracture strain rate than those closer to the bottom right corner. More details on using this chart are

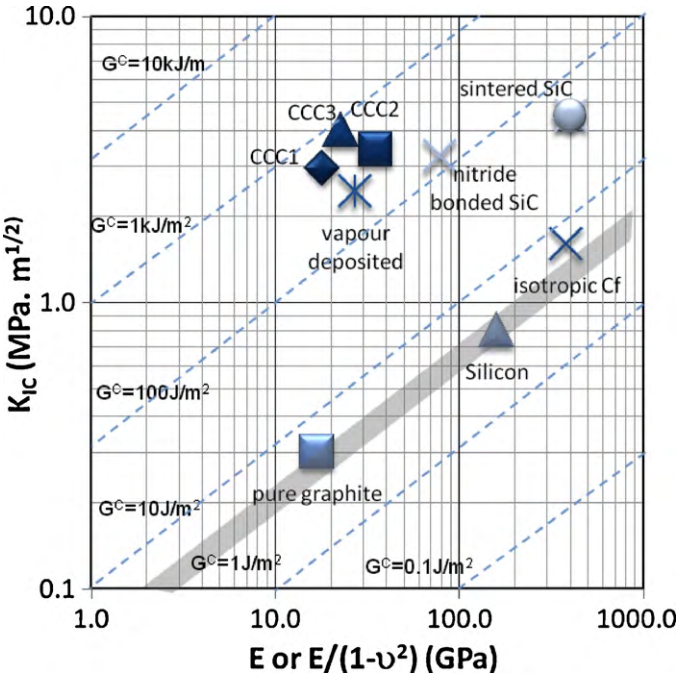

Fig. 12. Fracture toughness of ceramics (K_{IC}) plotted against Young's modulus (E, or $E/(1-\nu^2)$). The family of lines are of critical energy releasing rate (G^C). The shaded band shows that pure graphite, silicon and isotropic carbon fibres have same fracture energy; any ceramics above this band are more resistant to cracking than those on/below the band.

available from Ref. 17. Data drawn from Cambridge Materials Selection database[18] have been marked in this chart for these ceramics that could be comparable with the ceramic constituents observed in this composite: silicon, sintered SiC, nitride bonded SiC, vapour deposited SiC, pure graphite, isotropic carbon fibre. Three carbon fibre reinforced carbon composites (CCC1, CCC2 and CCC3) have also been included.[19] As shown in Fig. 12, silicon and graphite have the similar fracture strain rate, but much lower than any SiC ceramics and C_f/C composites. This implies that cracking damage would not have occurred in SiC and C_f/C regions when no cracking is observed in silicon. The discrepancy between the experimentally observed and theoretically predicted on the fracture resistance of the ceramic constituents during braking may imply that K_{IC} values measured from ceramics might have over-estimated, when these data are intended to be applied to measure the micro-cracking resistance of the constituents on the friction surface during braking. In fact, fracture resistance of polycrystalline ceramics could increase with crack extension, i.e. the well-known R-curve behaviour, and the magnitude of this increase could be in excess of a factor of three.[20] For ceramics with complex microstructure, like polycrystalline and composites, this difference would become more significant.[21]

Nevertheless, we think Fig. 12 could provide a guideline for understanding, designing and engineering these ceramic constituents for better friction performance of the composites, if the K_{IC} values are measured to genuinely gauge the resistance of microcracking or cracking initiation, rather than large crack propagation. Now, we believe that the following possibilities inside the silicon carbide might have led its surface more fragile than silicon: (a) the silicon carbide regions in the composite might have been weakly bonded as the grain boundaries were not purposely engineered in the LSI process, which could lead to a degradation of fracture toughness at the microstructure level, which was shown a possibility of less than 2.1 MPa $m^{1/2}$ by Padture and Lawn[22]; (b) large residual tensile stress could exist on the grains boundaries due to the constraint on the growth of silicon carbide grains in LSI process and the thermal strains generated during cooling down from the silicon impregnation temperature, which are featured through the appearance of stacking fault inside the SiC grains.[23,24] This view has been demonstrated in a study on the wear resistance of alumina, where the damage resistance has little relationship with large crack propagation resistance, i.e. K_{IC} measured by most methods, but a strong relationship with short crack energy releasing rate.[25] The same analysis can apply to C_f/C region where the short-crack energy releasing rate, particularly along the interface between carbon fibre and carbon matrix, should be significantly smaller than those measured from C_f/C composites or typical graphite, since in the design of most fibre reinforced composites, the fibre/matrix interfaces are deliberately weakened to improved the fracture tolerance,[26] which is why the three CCC composites, shown in Fig. 12, are sitting above all SiC ceramics. Unfortunately little experimental measurement is available on the interface or grain boundary fracture energy, as an addition in Fig. 12 to exhibit the picture more clearly. However, we are convinced through the analysis that short crack initiating or micro-crack propagating resistance must be improved for the ceramic matrix, including all interfaces in these composites in order to promote the development of a steady friction surface during braking for the aim of maintaining the friction and engineering performance of the composites, in addition to improve the adhesion of the third body materials on the friction surface.

4.3. Coefficient of friction and friction surface development

The development of these three types of friction surfaces on the surface of the composites could make a direct impact on the measurements of coefficient of friction and its stabilization. The growth of type I likely leads to a stable friction, and type II to a unstable friction; type III hardly gives an unstable friction, but its amount on the examined surface may be too small to give any significant influence in this study. In general, the growth of the transferred layer with the addition of further brakings increases the contact area between the disc and the pad; such an increment should lead to an improvement of the measured COFs, as shown in Fig. 2. Once the development of the transfer layer is stabilized, the COF would reach to a constant value, where it is generally regarded as the completion of bedding process. However, this stabilization has not yet been seen in Fig. 2 under the current testing regime. Judging from the development of the transfer layer on different regions, we believe that those on the silicon regions could give a stabilized state very swiftly, but much longer time is needed for those on the silicon carbide and C_f/C regions. Therefore, this unstable type II transfer layer could be the key factor that leaves C_f/C-SiC composite longer bedded-in time in a friction brake. In the tested composite, majority of the surface is

composed of C_f/C and SiC, and Si is less than 10%; the friction surface is hence dominated with type II friction surface. We envisage it would take longer time to achieve a stable coefficient of friction.

5. Summary

The development of friction transfer layer is studied on the friction surface of C_f/C-SiC composite when the composite disc is coupled with an organic pad. The transfer layer is composed of third body materials containing iron and copper as the main chemical elements; its development during friction strongly depends on the adhesion between the transferred materials and the ceramic matrix, as well as the steadiness of the ceramic substrate. Three types of friction surface are identified on the composite's surface: type I – the friction transferred layer has a steady relationship with the matrix and good longevity; type II – that the friction transferred layer has an unstable relationship with the matrix and poor durability; type III – the friction transferred layer has a steady relationship with the matrix but short lifetime. It appears that type I exists on all silicon regions and some silicon carbide regions; type II on all C_f/C regions and most of silicon carbide regions; type III in large voids and cracks/crevices.

The measured coefficients of friction show an increasing trend with the accumulation of braking stops, but did not yet reach to a stabilized level in the current test regime. These measurements echo the fact of friction surface development: the appearance of type I likely leads to a steady increase in COF swiftly, but the type II to an unstable friction and longer braking time to approach a stable level. One of the controlling factors for type II layer should be the fracture resistance of the matrix, apart from the adhesion strength between the transferred materials and the ceramic matrix. To avoid the appearance of type II surface, it is necessary to increase the critical strain rate of short crack propagation of silicon carbide and C_f/C regions in the composites.

Acknowledgements

The authors would like to acknowledge the EPSRC and the Technology Strategy Board in UK for providing studentship for YW. Mr. J. Bates and Dr. D. Ross are acknowledged for their technical support on using FEGSEM and MEF3 microscopy.

References

1. Krenkel W, Heidenreich B, Renz R. C/C-SiC composites for advanced friction system. *Adv Eng Mater* 2002;**4**(7):427–36.
2. Fan S, Zhang L, Xu Y, Cheng L, Lou J, Zhang J, et al. Microstructure and properties of 3D needle-punched carbon/silicon carbide brake materials. *Compos Sci Eng* 2007;**67**(11–12):2390–8.
3. Xu Y, Zhang Y, Cheng L, Zhang L, Lou J, Zhang J. Preparation and friction behaviour of carbon fibre reinforced silicon carbide matrix composites. *Ceram Int* 2007;**33**(3):439–45.
4. Krenkel W. Carbon fibre reinforced CMC for high-performance structures. *Int J Appl Ceram Technol* 2004;**1**(2):188–200.
5. Wang J, Jin Z, Qiao G. Rapid fabrication of C/C-SiC composites. *Key Eng Mater* 2006;**317–318**:159–62.
6. Cai YC, Xu Y, Li B, Fan S, Zhang L, Cheng L, et al. Low-cost preparation and frictional behavious of a three-dimensional needled carbon/silicon carbide composites. *J Eur Ceram Soc* 2009;**29**(3):497–503.
7. Zhang Y, Xu Y, Lou J, Zhang L, Cheng L. Braking behaviour of C/SiC composites prepared by chemical vapour infiltration. *Int J Appl Ceram Technol* 2005;**2**(2):114–21.
8. Jiang G, Yang J, Xu Y, Gao J, Zhang J, Zhang L, et al. Effect of graphitization on microstructure and tribology properties of C/SiC composites prepared by reactive melt infiltration. *Compos Sci Technol* 2008;**68**(12):2468–73.
9. Krenkel W, Berndt F. C/C-SiC composites for space applications and advanced friction system. *Mater Sci Eng* 2005;**A412**(1–2):177–81.
10. Stadler Z, Krnel K, Kosmac T. Friction behaviour of sintered metallic brake pads on a C/C-SiC composite brake disc. *J Eur Ceram Soc* 2007;**27**(2–3):1411–7.
11. Liu T, Rhee SK, Lawson KL. A study of wear rates and transfer films of friction materials. *Wear* 1980;**60**(1):1–12.
12. Paris JY, Vincent L, Denape J. High-speed tribological behaviours of carbon/silicon-carbide composite. *Compos Sci Technol* 2001;**61**(3):417–23.
13. Godet M, Play D, Berthe D. An attempt to provide a uniform theory of tribology through load-carrying capacity, transport and continuum mechanics. *J Lubr Technol* 1980;**102**(2):153–64.
14. Österle W, Griepentrog M, Gross T, Urban I. Chemical and microstructural changes induced by friction and wear of brakes. *Wear* 2001;**251**:1469–76.
15. Österle W, Urban I. Third body formation on brake pads and rotors. *Tribol Int* 2006;**39**:401–8.
16. Wang Y, Wu H, unpublished work.
17. Ashby MF. *Materials selection in mechanical design*. 3rd ed. Oxford: Elsevier; 2008. pp. 45–78.
18. *Cambridge Engineering Selector, Version 5.1.0*. Granta Design Ltd.; 2009.
19. Lackey WJ. In: Buschow KHL, Cahn R, et al., editors. *Encyclopaedia of materials: science & technology*. Elsevier Science Ltd.; 2001. p. 952–67.
20. Cook RF, Lawn BR, Fairbanks CJ. Microstructure-strength properties in ceramics. I. Effect of crack size on toughness. *J Am Ceram Soc* 1985;**68**(11):604–15.
21. Bennison SJ, Lawn BR. Role of interfacial grain-bridging sliding friction in the crack-resistance and strength properties of nontransforming ceramics. *Acta Metal* 1989;**37**(10):2659–71.
22. Padture NP, Lawn BR. Toughness properties of a silicon carbide with an in situ induced heterogeneous grain structure. *J Am Ceram Soc* 1994;**77**(10):2518–22.
23. Lawn BR. *Fracture of brittle solids*. 2nd ed. Cambridge, U.K: Cambridge University Press; 1993. pp. 319–24.
24. Leatherborrow A, Wu H. The nature of silicon carbide phases developed from different carbonaceous sources and its impact on the microstructure of C_f/C-SiC composites. In: *Proc 34th Int Conf & Exp on Adv Ceram Eng Sci Proc* 31 (8), in press.
25. Cho SJ, Hockey BJ, Lawn BR, Bennison SJ. Grain-size and R-curve effects in the abrasive wear of alumina. *J Am Ceram Soc* 1989;**72**(7):1249–52.
26. Hull D, Clyne TW. An introduction to composite materials. In: *Cambridge solid state science series.* 2nd ed. Cambridge: Cambridge University Press; 1996. pp. 147–53.